molecular pharmaceutics

ARTICLE

pubs.acs.org/molecularpharmaceutics

Insights into the Early Dissolution Events of Amlodipine Using UV Imaging and Raman Spectroscopy

Johan P. Boetker,[†] Marja Savolainen,[†] Vishal Koradia,[†,‡] Fang Tian,[†] Thomas Rades,[§] Anette Müllertz,[†] Claus Cornett,[†] Jukka Rantanen,[†] and Jesper Østergaard[*,†]

[†]Department of Pharmaceutics and Analytical Chemistry, Faculty of Pharmaceutical Sciences, University of Copenhagen, Universitetsparken 2, 2100 Copenhagen, Denmark

[§]School of Pharmacy, University of Otago, 18 Frederick Street, Dunedin 9054, New Zealand

Supporting Information

ABSTRACT: Traditional dissolution testing determines drug release to the bulk, but does not enable an understanding of the events happening close to the surface of a solid or a tablet. UV imaging is a new imaging approach that can be used to study the dissolution behavior of chemical compounds. The UV imaging instrumentation offers recording of absorbance maps with a high spatial and temporal resolution which facilitates the abundant collection of information regarding the evolving solution concentrations. In this study, UV imaging was used to visualize the dissolution behavior of amlodipine besylate (amorphous and dihydrate forms) and amlodipine free base. The dissolution of amlodipine besylate was faster from the amorphous form than from the crystalline forms. The UV imaging investigations suggested that a solvent mediated phase transformation occurred for the amorphous amlodipine besylate and the amlodipine free base samples. Raman spectroscopy was used to confirm and probe the changes at the solid surface occurring upon contact with the dissolution media and verified the recrystallization of the amorphous form to the monohydrate. The combination of UV imaging and Raman spectroscopy is an efficient tool to obtain a deeper insight into the early events of the dissolution process.

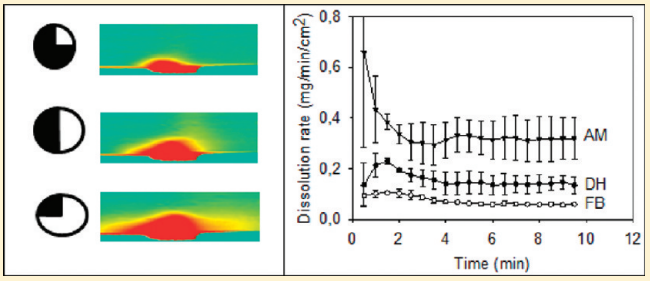

KEYWORDS: amorphous, crystalline, dissolution, Raman spectroscopy, solid-state transformation, UV imaging

INTRODUCTION

The increasing number of poorly water-soluble drug candidates has sparked a high interest in exploring formulation approaches involving the optimization of solid-state properties including the use of high energy solid forms such as amorphous systems, solid dispersions or different polymorphs, in order to increase the dissolution rate. These systems often contain thermodynamically metastable or even unstable forms of the active ingredient, and a full understanding of the factors affecting product performance can be challenging.[1,2] When the surface of such systems is exposed to a solvent, phase transformations may occur.[3−5] Furthermore, the drug release from such samples is often governed by a complex interplay between dissolution and recrystallization (nucleation and crystal growth). This behavior may be further complicated by pH effects, surfactants, ions and other components present in the gastrointestinal (GI) tract.[6,7] The development of bio- and physicochemically relevant dissolution methods is therefore important to better understand and predict dosage form performance.[6−17]

Traditional dissolution testing methodologies are based solely on bulk solution concentration measurements as a function of time.[18,19] These approaches suffer from delayed responses due to the need for accumulation of the solution concentration. The absence of simultaneous real-time information regarding the solution concentration and the solid-state composition makes the detection of solid-state changes during dissolution difficult since these often commence almost instantaneously.[20] Hence, the lack of real-time information may preclude the possibility for understanding the behavior of a formulation. A recent editorial has underlined the necessity for the development of new analytical tools that can increase the understanding of complex dissolution behavior.[21] Imaging techniques such as FT-IR, NIR and magnetic resonance imaging (MRI) have been used for studying dissolution processes.[22−25] However, FT-IR and NIR imaging are water sensitive, restricting their use in aqueous media, although the utilization of attenuated total reflectance (ATR) accessories has enabled the investigation of aqueous solutions with FT-IR imaging.[26,27] Coherent anti-Stokes Raman scattering (CARS) for three-dimensional imaging is a new emerging technique.[28] CARS has recently been applied to imaging of lipid-based oral dosage forms.[29] However, CARS suffers from nonlinear concentration dependence,[30] and the quantitative interpretation of CARS imaging may be difficult when applied to nonlipid imaging.[31]

Received: April 19, 2011
Accepted: June 2, 2011
Revised: June 1, 2011
Published: June 02, 2011

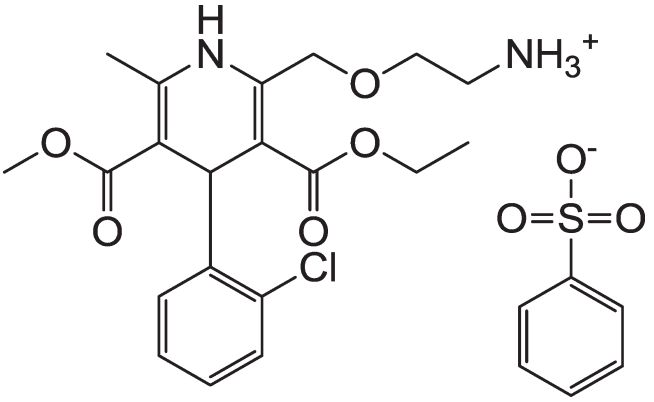

Figure 1. Chemical structure of amlodipine besylate.

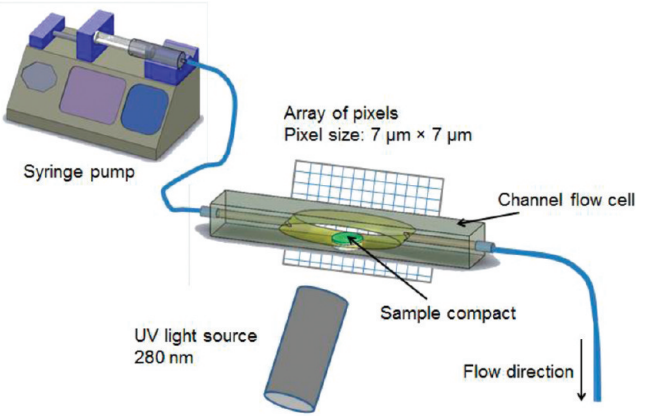

Figure 2. Schematic representation of the UV imaging setup.

The recent availability of UV imaging[32,33] may enable the visualization of solution concentrations around a given solid sample in real time. This provides a possibility to obtain new insights into the dissolution process and to capture the initial stages of the dissolution process which may be missed in traditional dissolution testing. During dissolution, local supersaturation may occur, and this can result in the nucleation and growth of a new solid form. These phase transformations are likely to affect the dissolution rate, since even a thin layer of a thermodynamically more stable form on the surface could change the dissolution rate of the drug to that of the more stable form.[34] In addition the transformation may also affect the surface area in a noncontrollable way, thus multiple phenomena may be occurring simultaneously.[20,35−37] UV imaging technology provides a platform for generating spatially and temporarily resolved solution phase information (absorbance maps) that may help elucidate these processes, and when this imaging technology is combined with the channel flow cell method, dissolution rates may be obtained. An additional benefit of the channel flow cell setup is the well-defined hydrodynamics and associated solute transport to the detection region.[38−41] Furthermore, previous studies have shown that Raman spectroscopy is an efficient approach for gaining a qualitative insight into these solid-state change phenomena in aqueous environments, such as conditions during dissolution testing.[20,42−47] Raman spectroscopy will therefore be utilized as a complementary technique to determine solid form changes.

The current study demonstrates the feasibility of UV imaging to monitor drug dissolution as well as associated (re)crystallization processes occurring during the dissolution of amlodipine and amlodipine besylate (Figure 1) in real time. Amlodipine besylate and its free base form were chosen as model systems since they occur in various solid forms and are known to undergo solvent mediated transformations.[48,49] Amlodipine dissolution from compacts was investigated by UV imaging under static conditions as well as in a channel flow mode.

EXPERIMENTAL SECTION

Materials. Amlodipine besylate anhydrate (AH) was obtained from Matrix Laboratories Limited (Secuderabad, India, batch no. ADP0140208, EP/USP grade). The monohydrate form (MH) was prepared by cooling crystallization from aqueous solution. AH was dissolved in water at 85 °C and stirred for 30 min. The resulting solution was cooled over an ice bath until the solution reached 5 °C. The crystals were collected by filtration. The dihydrate form (DH) was prepared from an aqueous slurry by stirring the AH crystals in water for 2 days at 25 °C. The crystals were collected by filtration and dried at 40 °C. The amorphous form (AM) was prepared by dehydration from the monohydrate. The MH was heated to 105 °C, and upon dehydration the melt was rapidly cooled in a freezer.[48] The obtained AM form was subsequently grinded. The free base form I (FB) was prepared from the AH by suspending the AH in 2-propanol follow by the addition of 1 M NaOH aqueous solution under stirring. The reaction mixture was cooled to 5 °C, and the solid was filtered off and dried in an oven at 40 °C. All solid-state forms were verified by XRPD. Ammonium acetate was purchased from Prolab (Leuven, Belgium). Ultrapure water was obtained from a Milli-Q plus system (Millipore, Milford, USA). The dissolution medium (acetic acid−acetate buffer pH 3.50, 3.24 mol/L) was prepared according to Ph. Eur. (4000600).

Methods. *UV Imaging Instrumentation.* UV imaging was performed using an Actipix SDI300 dissolution imaging system (Paraytec Ltd., York, U.K.) (Figure 2). The total imaging area is 9 mm × 7 mm (1280 × 1024 pixels). The quartz channel flow cell has a light path of 3.0 mm and holds a cell volume of ∼560 μL. The light source consists of a Xe lamp with an interchangeable wavelength filter, and imaging was performed at a single wavelength of 280 nm. Images were recorded (2.6 images per s, subsampling of every fifth image was applied) and analyzed with Actipix D100 software version 1.3 (Paraytec Ltd.). The pixels were binned in the horizontal direction in sets of 10 (10 × 1 pixel binning). A syringe pump was used for infusion of the dissolution medium. All experiments were carried out at ambient temperature (20 to 23 °C). UV imaging calibration curves were obtained by imaging of amlodipine besylate standard solutions (3.61×10^{-4}, 1.14×10^{-3}, 1.94×10^{-3}, 2.74×10^{-3}, 3.53×10^{-3} and 5.28×10^{-3} M) infused into the channel flow cell.

Preparation of Compacts. Compacts were made by weighing 6 mg of substance into a stainless steel cylinder (inner diameter: 2 mm) held in a manual press (Actipress, Paraytec Ltd.). A Quickset MINOR torque screwdriver (Torqueleader, M. H. H. Engineering Co. Ltd., England) was used to compress the amlodipine samples at a constant torque (pressure) of 0.12 N m.

Dissolution in the Absence of Flow. The general procedure for UV imaging was as follows: dark images (lamp turned off for 10 s) and reference images (10 s) were recorded with the channel flow cell filled with the acetic acid−acetate buffer pH 3.50 (dissolution medium). After 60 s of data collection, the recording

was paused, and the compact was inserted. During the reference period, a stainless steel cylinder was placed in the sample holder. After placing the compact containing either DH, FB or AM, data collection was resumed, and the channel flow cell was filled with dissolution medium (1 mL/min). The flow was arrested upon completion of the filling of the channel flow cell, and UV images were collected for 10 min in the absence of flow. All experiments were performed at least in triplicate.

Dissolution in the Presence of Flow. The dissolution of amlodipine solid forms in the presence of flow was essentially performed as the dissolution experiments under static conditions, except that after the channel flow cell was filled (1 mL/min) with dissolution medium, the flow was adjusted to 200 μL/min and UV images were subsequently collected for 10 min. The dissolution rate given at the defined time points (in 30 s intervals) was calculated using the Actipix D100 software version 1.3 (Paraytec Ltd.) by averaging over 15 frames. The software calculates the dissolution rate from the absorbance read from each pixel in the quantification region downstream to the sample surface. Each pixel row within this quantification region is associated with a flow velocity according to the parabolic flow profile inside the channel flow cell. These input values combined with the surface area of the compact, molar mass and molar absorptivity of the compound enable the software to calculate the dissolution rate for the compound. The imaging area selected for the quantitative analysis in the presence of flow was 0.5×2.5 mm^2.

Raman Spectroscopy. The solid compact samples were analyzed prior to and immediately after the UV imaging dissolution experiments using a Raman spectrometer (Control Development Inc., South Bend, IN, USA) equipped with a thermoelectrically cooled CCD detector and a fiber optic probe (InPhotonics, Norwood, MA, USA). The measurements were carried out at room temperature using a 500 mW laser source with a wavelength of 785 nm (Starbright 785S, Torsana Laser Technologies, Skodsborg, Denmark). The integration time was 3 s, and each spectrum was an average of 8 scans.

The kinetics of the solution mediated phase transformation of amlodipine besylate from the AM form to the MH form was studied by exposing an AM sample to the dissolution medium and subsequently taking a Raman spectrum every 20 s for 10 min. The resulting spectra were analyzed using principal component analysis (PCA). The PCA was performed on the Raman spectra using the 940 to 1685 cm^{-1} spectral region. Before PCA standard normal variant (SNV) transformation was performed to remove intensity differences unrelated to the sample composition and the spectra were subsequently mean centered. PCA, preprocessing and scaling were performed using the PLS toolbox version 6.0.1 (eigenvector Research Inc., Wenatchee, WA, USA) installed on Matlab version 7.11.0.584 2010b (Natick, MA, USA).

Differential Scanning Calorimetry (DSC). DSC measurements were done using a Perkin-Elmer DSC 7 (Perkin-Elmer, Norwich, CT, USA) controlled by Pyris software (version 7.0.0.0110). The temperature axis and heat flow of the equipment were calibrated using indium. Samples (3.5−5 mg) were analyzed in crimped 40 μL pans with pin holed 50 μL lids. Measurements were carried out at a heating rate of 10 K/min under a nitrogen flow of 20 mL/min.

Thermogravimetric Analysis (TGA). TGA measurements were done using a Perkin-Elmer TGA 7 (Perkin-Elmer, Norwich, CT, USA) controlled by Pyris software (version 7.0.0.0110). Samples (5−6 mg) were analyzed in a flame-cleansed platinum pan under open conditions at a heating rate of 10 K/min under a nitrogen flow of 20 mL/min.

Nuclear Magnetic Resonance (NMR). ^{1}H NMR measurements were acquired using a Bruker Avance av400 WB (Bruker, Rheinstetten, Germany) operating at 400.13 MHz for ^{1}H. Prior to analysis samples were dissolved in dimethyl sulfoxide (DMSO). Spectra were acquired into data points in the time domain using a 30 degree pulse and a relaxation delay of 15 s. Sixteen transients were added. The spectra were apodized with an exponential function, corresponding to 0.30 Hz line broadening, and Fourier transformed into 65536 data points.

X-ray Powder Diffraction (XRPD). XRPD were measured on a PANalytical X'Pert Pro θ/θ diffractometer equipped with a PIXcel detector (PANalytical B.V., Almelo, The Netherlands). A continuous 2θ scan was performed in a range of 2° to 40° using Cu Kα radiation (λ = 1.5418 Å) with a step size of 0.0390° 2θ and a speed of 0.05° 2θ/s. Kβ radiation was eliminated by a nickel filter. The voltage and current applied were 45 kV and 40 mA, respectively. Sample spinning was performed during measurements to limit the effect from preferred orientation. Data were collected using X'Pert data collector version 2.2 and analyzed with X'Pert highscore plus version 2.2.4 (both from PANanalytical B.V., Almelo, The Netherlands).

UV Spectrophotometry. UV absorbance spectra were obtained for both amlodipine besylate and amlodipine free base by dissolving each solid form in the dissolution media and performing an absorbance scan using a conventional double beam spectrophotometer (Evolution 300, Thermo scientific, Madison, WI, USA).

Light Microscopy. The solid samples were analyzed prior to and after dissolution experiments using a light microscope (Zeiss Discovery V8 Stereo, Carl Zeiss AG, Jena, Germany) equipped with a Axiocam ICc camera and Axiovision 40 (Version 4.8.2.0.) software utilizing 4× magnification.

RESULTS

Initial UV Imaging Experiments. The UV imaging experiments were conducted at ambient temperature (20−23 °C) due to the lack of a suitable means for controlling temperature at the time of the experiments (a solution has since been provided by the instrument manufacturer). Consequently, the equilibrium solubility of dihydrate amlodipine besylate was determined to $4.6 \times 10^{-3} \pm 9.9 \times 10^{-5}$ M and $5.3 \times 10^{-3} \pm 3.5 \times 10^{-5}$ M in the acetic acid−acetate buffer (pH 3.50) at 20 °C and 23 °C , respectively (n = 3). The solubility at 20 °C was ∼13% lower than at 23 °C; thus some variability in the dissolution experiments may be encountered due to the variation in temperature. The spectra were anodized with an exponential function (line broadening $0.30H_2$) and Fourier transformed into 65536 data points.

The UV imaging instrumentation applied allows detection at a single wavelength at a time only. Amlodipine besylate is completely dissociated in aqueous solution and has UV absorbance maxima at 243 and 366 nm in the acetic acid−acetate buffer applied (see Figure S1 in the Supporting Information). However, initial UV imaging experiments of amlodipine besylate dissolution indicated that detection at these wavelengths would provide absorbance values well above the linear range of Beer's law. A detection wavelength of 280 nm, which is positioned near a local minimum in the absorbance spectrum, was selected on the basis of these requirements and filter options available in the lab. Separate UV absorbance measurements showed that the absorption coefficient at 280 nm was the same for the amlodipine besylate AH and amlodipine FB.

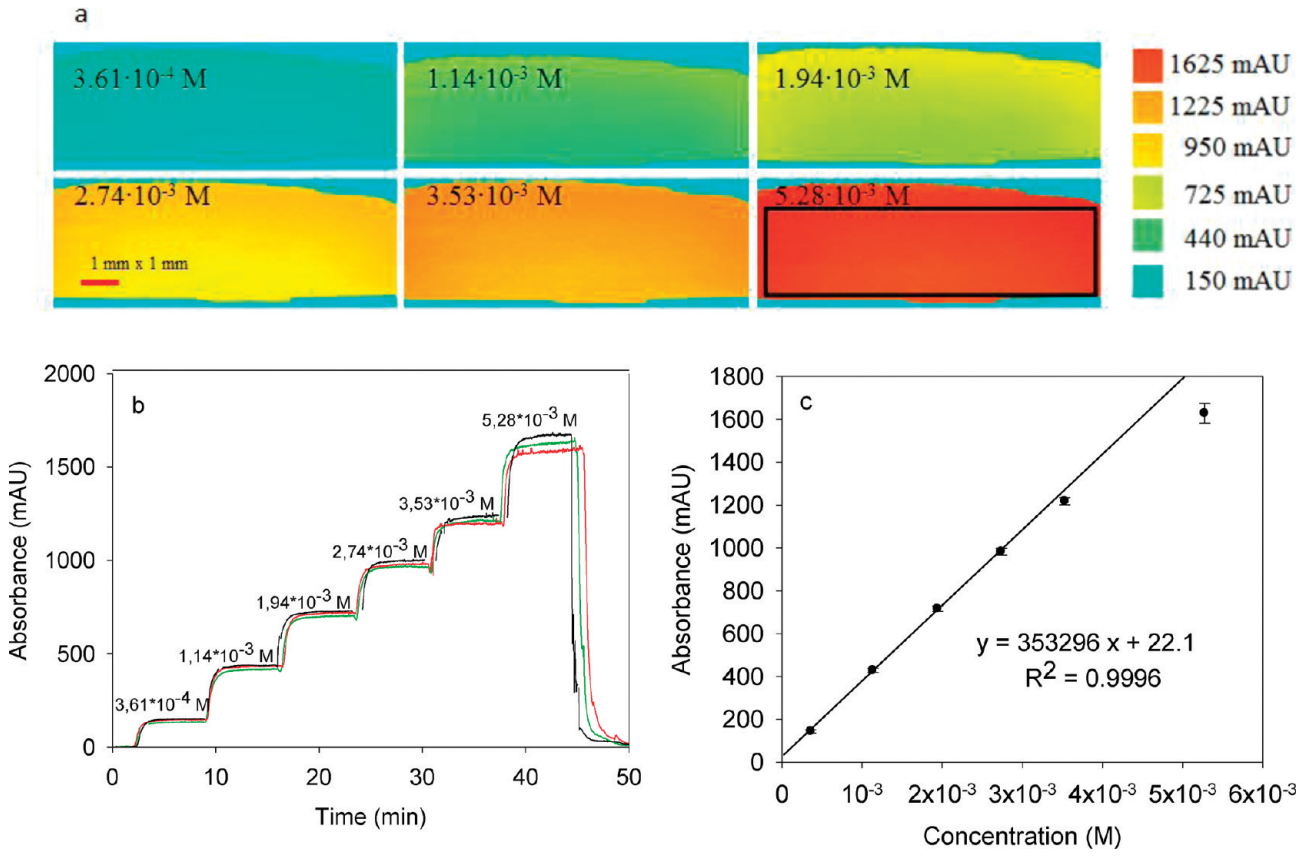

Figure 3. UV imaging of amlodipine besylate standard solutions at 280 nm in acetate buffer (pH 3.50). (a) UV absorbance maps obtained by consecutively flowing amlodipine besylate standards through the channel flow cell. (b) Average UV absorbance−time profiles obtained by flowing standard solutions through the cell (n = 3). The absorbance values were obtained by averaging the pixels within the area of the box in panel a. (c) Calibration curve constructed from plateau absorbance values. Error bars represent the standard deviation (n = 3), and the solid line was obtained by linear regression analysis using the 4 lowest concentrations.

A calibration curve was obtained for the UV imaging system by imaging standard solutions. The concentration of the standard solutions can be visualized by the absorbance maps (Figure 3a). The intense red color indicates a high absorbance and hence high concentration.

The solutions were infused consecutively starting with the lowest concentration and ending with the highest concentration and repeated three times (Figure 3b).

A calibration curve (Figure 3c) was established using the plateau absorbance values shown in Figure 3b. The standard curve shows significant deviation from linearity above 1000 mAU (Figure 3c). The molar absorptivity ε_{280} was calculated to be 120 m^2/mol using the first 4 points of the standard curve. The sensitivity of the UV imaging method was estimated as the capability to discriminate between concentration differences to be 5.0×10^{-5} M using eq S2 in the Supporting Information.

Dissolution Imaging at Static Conditions. Three different forms of amlodipine were evaluated using UV imaging under static conditions. Figure 4 shows the absorbance map at different time points, where intense red color indicates high absorbance values and the contours depict lines with similar absorbance. The outer contour line has a value of 400 mAU, which is equivalent to a 1.0×10^{-3} M solution concentration of amlodipine.

It was observed from the absorbance maps that the DH sample has a slower dissolution than the AM sample. This slower dissolution of the DH sample is visualized directly by the smaller area spanned by the DH sample contour lines (Figure 4). This was expected because the DH sample is the stable form of amlodipine besylate under aqueous conditions.[48] Density gradients in the vicinity of the surface of the dissolving sample are most likely affecting the local solution concentration distribution within the cell. Accumulation of dissolved amlodipine is primarily occurring in the lower part of the UV images for the DH sample due to a higher density of the solution as compared to the solvent (Figure 4a). This pattern is less predominant for the FB sample which, together with the AM sample, has contour lines that experience a distinct vertical shift in the center of the UV images (red arrows in Figure 4). This apparent upward shift is caused by a change in the surface height of the sample, and thereby indicates growth of crystalline material on the surface of the AM and FB samples. Inspection of the recorded images clearly shows that the changes in absorbance as a function of time are not compatible with the transport of amlodipine by diffusion. Sudden changes in absorbance were observed, indicating the growth of solid material. This was also apparent from light microscopy (Figure 5a−c) and visual inspection of the compacts within the channel flow cell (Figure 5d), where a change from a smooth surface appearances to shapes that extended beyond the boundaries of the cylindrical compacts was observed (red arrows in Figure 5 and inset) for both AM and FB but not for the DH samples.

Dissolution Imaging in the Presence of Flow. The dissolution of the three forms of amlodipine was subsequently evaluated

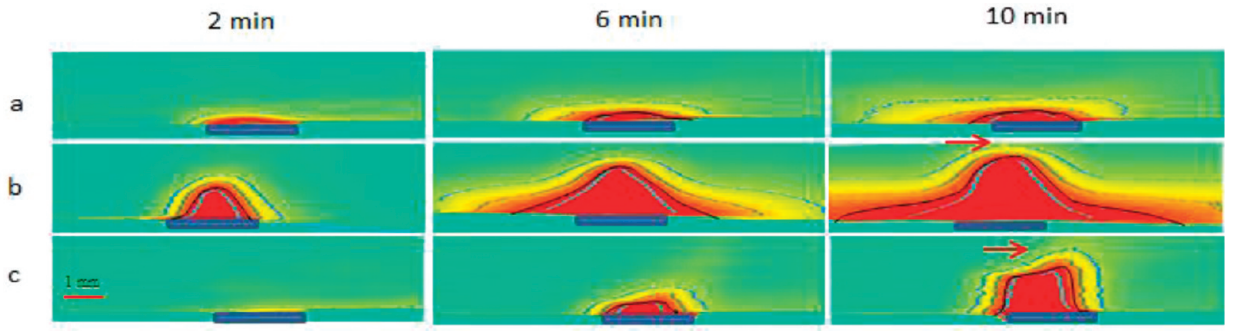

Figure 4. UV absorbance maps of dissolution at static conditions of (a) amlodipine besylate dihydrate, (b) amorphous amlodipine besylate and (c) amlodipine free base. Contour lines: blue, 400 mAU, green, 800 mAU, black, 1200 mAU and light blue, 1600 mAU. The significance of the arrows is explained in the text.

by UV imaging while applying a continuous flow of 200 μL/min. The UV imaging data indicated that the AM and FB samples were subject to precipitation of solid material (Figure 6) which was observed as a crystal growth from the compact surface. Again, this crystal growth, on top of the sample surface, can be deduced from the UV images as the blocking of the light path by the solid material in the AM and FB samples and was also seen from light microscopy. However, under flow conditions the blocking of the light path above the solid sample compact in itself has no influence on the determination of the absorbance due to the dissolved drug substance because this is calculated from the downstream selection of pixels spanned by the inserted rectangular box (Figure 6). It is noted that quantitative analysis, here in terms of dissolution rates, can be performed irrespective that a different pixel area was utilized for the determination of the molar absorptivity, since it has previously been demonstrated that different pixel areas within the absorbance map provide similar absorbance values (relative standard deviation <0.3%).[32] In the experiments where crystal growth on the sample surface is occurring, the accuracy of the determined dissolution rates relies on the assumption that the flow profile is unaltered by the deposited material or restored prior to reaching the quantification region.

It should be noted that the measured absorbance values in the depicted quantification area were all within the linear range of the calibration curve (below 1000 mAU). Furthermore, the anticipated well-defined laminar channel flow hydrodynamics does not appear to be significantly impaired by the growth of solid on the sample surface. This is seen by evaluating the width of the absorbance pattern of the dissolved drug that effectively works as a flow tracer[50] (inset in Figure 6d). The UV image excerpts in Figure 6 also provide a visual representation and a means for the qualitative assessment of differences in dissolution rates for the investigated solid forms. From the absorbance maps it is apparent that the dissolution rates at 10 min increase in the order FB < DH < AM.

Figure 7 displays the dissolution rates for the three solid forms which were calculated using the known flow rate, measured concentration in the specified pixel area and surface area of the compact. It is apparent that the FB has the lowest dissolution rate after 1 min and the DH exhibited an intermediate dissolution rate. Both the DH and FB samples initially showed a high dissolution rate that declined after 2 min. The AM samples were found to have the highest dissolution rate throughout the experiment, irrespective of the relatively large decrease in the dissolution rate that is initially apparent. The larger variability

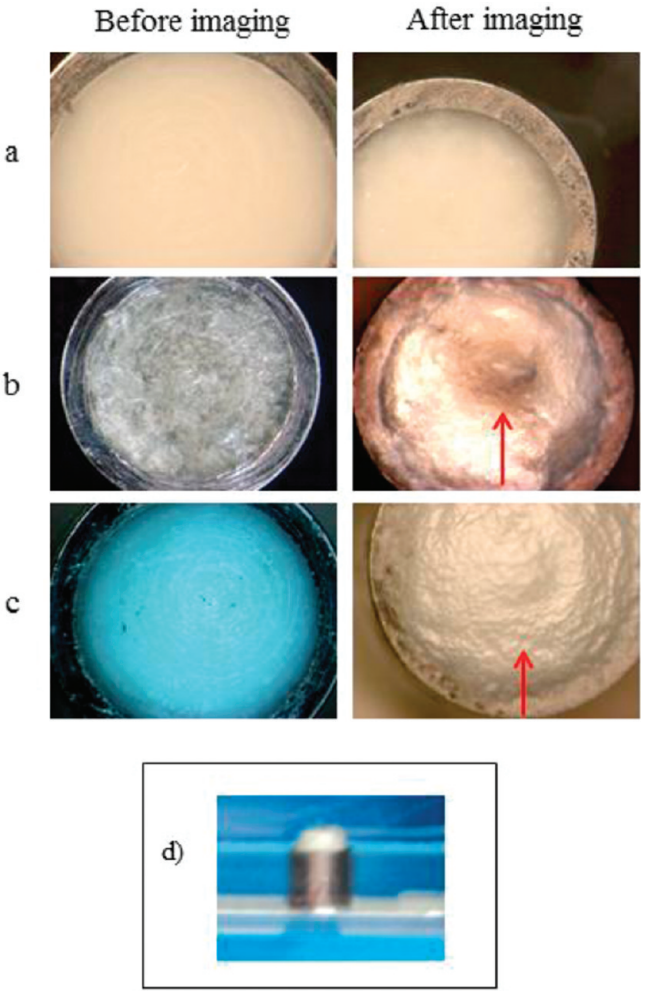

Figure 5. Light microscopy photographs of the compacts containing (a) amlodipine besylate dihydrate, (b) amorphous amlodipine besylate and (c) amlodipine free base prior to and after imaging. The red arrows indicate crystal growth beyond the boundaries of the cylindrical compact. (d) Representative photo of compact within the channel flow cell showing crystal growth of amorphous amlodipine besylate upon dissolution imaging at static conditions.

with respect to the dissolution rate (apparent from the standard deviations in Figure 7) encountered for the dissolution experiments involving the amorphous amlodipine besylate is speculated

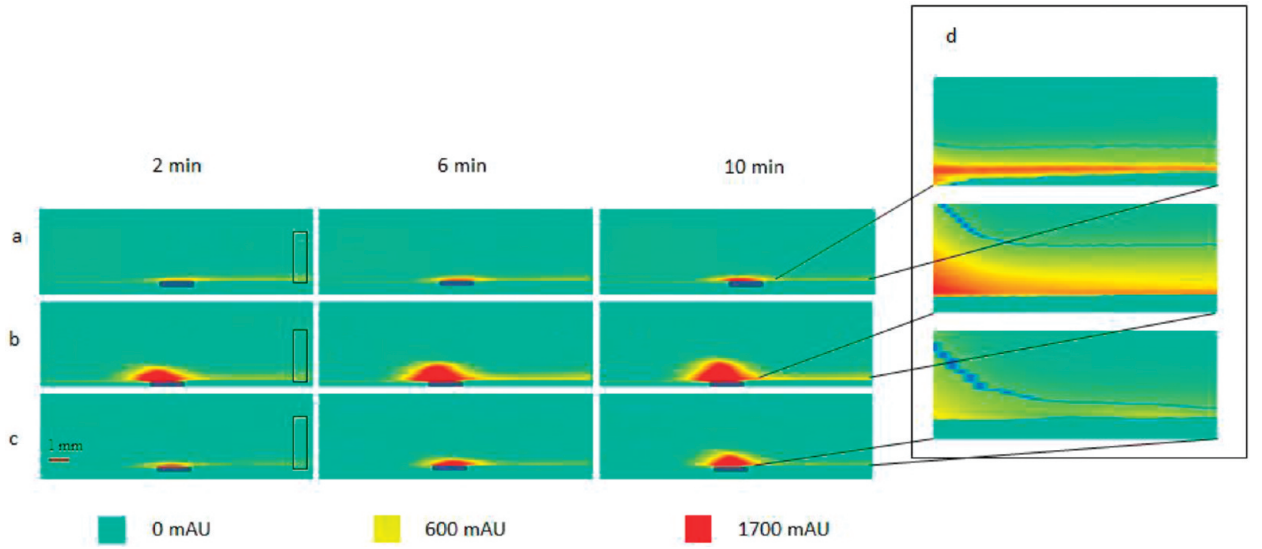

Figure 6. UV absorbance maps of dissolution at flow conditions (200 μL/min) of (a) amlodipine besylate dihydrate, (b) amorphous amlodipine besylate, (c) amlodipine free base. The insets (d) show the spatially resolved concentration distribution downstream from the sample. Contour line: blue, 200 mAU.

to be due to the stochastic nature of the crystallization process which makes the exact onset of nucleation unpredictable. The standard deviations related to the crystalline forms were remarkably smaller (Figure 7).

Solid Phase Transformations during Dissolution Testing. Raman spectroscopy was used prior to and after UV imaging to characterize the solid state. It has previously been demonstrated that Raman spectroscopy is capable of obtaining root-mean-square error of prediction (RMSEP) values of $\leq$2.6%.[51] The Raman spectra of the various amlodipine besylate forms were in accordance with those previously published.[48] Based on the analysis using Raman spectroscopy, no solid-state transformation was observed during the dissolution experiments for the crystalline DH form. This was as expected, because the DH is the thermodynamically stable form in aqueous solutions.[48]

Figure 8 shows changes in the Raman spectra for the AM samples after 10 min of contact with the dissolution media. For example, a peak shift from 1038 cm^{-1} to 1045 cm^{-1} occurred (red line, Figure 8b) which can be assigned to the 1,2-substituted phenyl ring (Figure 1).[52] This peak shift corresponds to the conversion of the AM to the MH form and can be used to monitor the solid-state transformation. Further conversion from the MH to the DH form was not observed within the duration of the experiment, which is in accordance with previous findings. The kinetics of this transformation has been reported to be relatively slow, occurring after 19 h of contact with the aqueous medium at 37 °C .[48]

The transformation time for the conversion of the AM form to MH form was subsequently evaluated by immersing an AM sample into the dissolution medium and obtaining a Raman spectrum every 20 s. These spectra were then compared with MH and AM reference spectra using PCA. The PCA plot in Figure 9a utilized 3 components to explain 79% of the variation in the data set. It is observed that the amorphous starting sample (green) is situated far away from the crystalline MH reference sample (red).

Furthermore, it is seen that the remaining time points are moving toward the MH reference sample (Figure 9a). The PCA plot therefore shows that the transformation from the AM form to

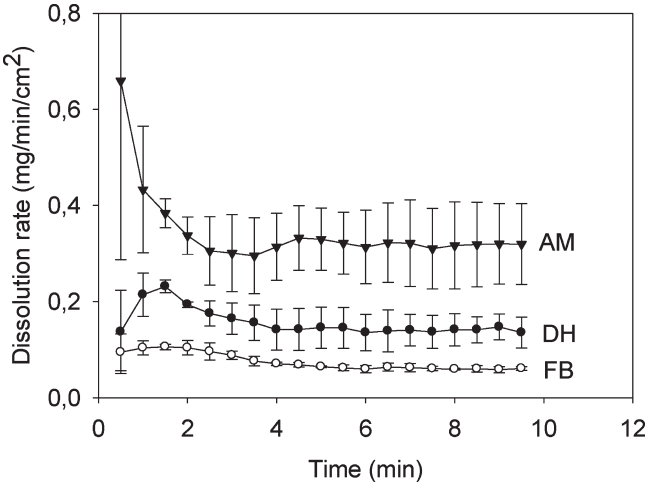

Figure 7. Dissolution rates of amorphous amlodipine besylate (AM), amlodipine besylate dihydrate (DH) and amlodipine free base (FB) as a function of time obtained by UV imaging at a flow rate of 200 μL/min. Error bars represent the standard deviation (n = 3).

the MH form commences almost instantaneously after exposure to the dissolution medium which is in line with the UV imaging results. The score plot is primarily using PC 1 to discriminate between the AM, MH and various time points in between (0.3 to 10.2 min) which is seen as peak shifts at 1000, 1040, and 1130 cm^{-1} in the loading vector of PC1 (Figure 9b). PC 2 is primarily used to separate the various time points according to the peak intensity at 1000, 1590, and 1650 cm^{-1} (Figure 9b).

Raman shifts were also noted for the FB after imaging. However, DSC and XRPD experiments (Figures S2 and S3 in the Supporting Information, respectively) indicated that the resulting product did not match any of the two reported FB forms (form I and II).[53] The FB form I was subsequently dissolved in the acetic acid−acetate buffered dissolution medium and stirred for 8 h at ambient temperature. The resulting precipitate was filtered off and dried in an oven at 40 °C for 1 day.

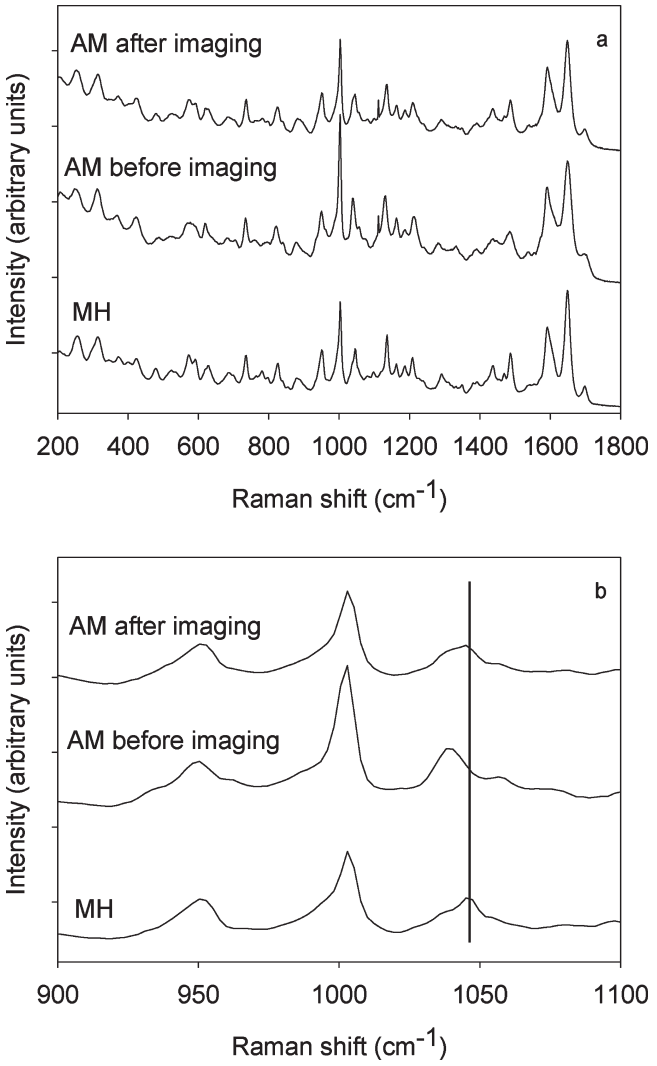

Figure 8. (a) Raman spectra of the amorphous amlodipine besylate (AM) sample before and after UV imaging and amlodipine besylate monohydrate reference spectrum (MH). (b) Magnification of the Raman spectral region 900 cm^{-1} to 1100 cm^{-1}. Red line at 1045 cm^{-1}.

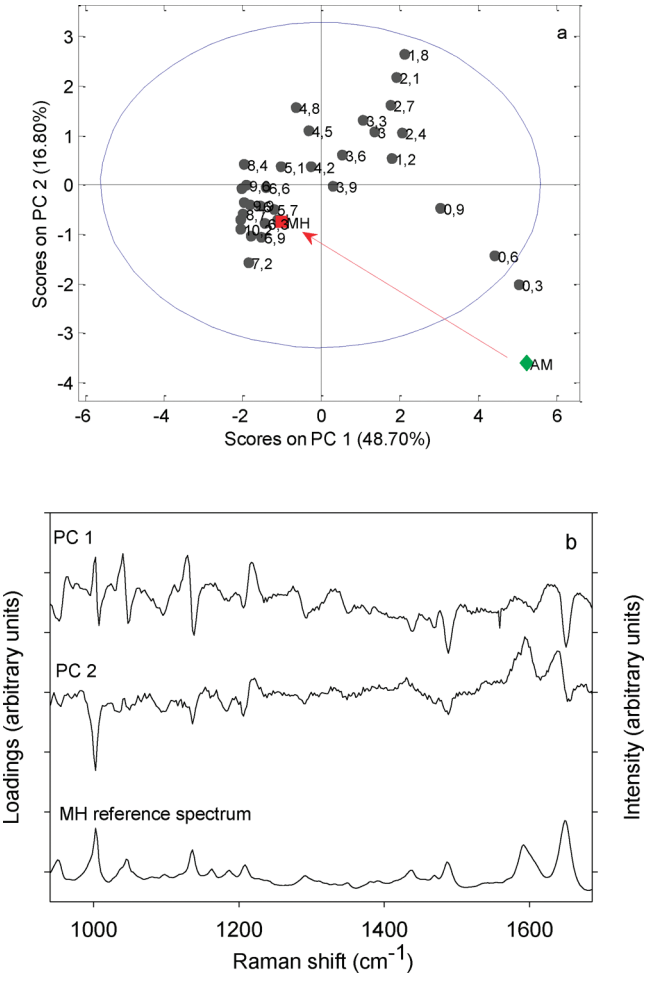

Figure 9. (a) PCA score plot of Raman spectra: red ■, reference monohydrate (MH); green ◆, amorphous amlodipine besylate (AM). Numbers correspond to time points given in minutes. Red arrow: tendency line. (b) Loadings on PC 1 and PC 2 for Raman data and reference spectrum of monohydrate (MH).

NMR performed on this product confirmed that the FB did not undergo any chemical reaction (Figure S4 in the Supporting Information) and TGA showed a weight loss (Figure S5 in the Supporting Information). It is therefore suggested that a solvate was formed; a detailed investigation of this new form was considered beyond the scope of the present study.

■ DISCUSSION

The AM and FB samples recrystallized during the dissolution experiments, and an increase in surface area was observed which was indirectly apparent from the UV imaging data (Figure 4). Such a growth in surface area was not observed for the DH samples, indicating that solvent mediated transformation did not occur for this form. These observations were verified by Raman spectroscopy. Our initial studies indicate that UV imaging may be capable of detecting solvent mediated solid-state transformations. In the absence of flow (static conditions), the quantification of the amount of dissolved drug from AM and FB samples was impeded by the elevated absorbance values stemming from either the solution concentration itself, precipitation of solid material that was obstructing the light transmission path or a combination[54] of both. Experiments conducted using a higher wavelength, where the dissolved amlodipine besylate does not absorb light, may in the future be helpful in discriminating between solid material and material in solution at static conditions.

Furthermore, the UV imaging equipment enables visualization from the very onset of a dissolution experiment and thus provides a new insight into early dissolution phenomena. The UV imaging equipment also provides direct information about the initial dissolution rates which was in the order AM > DH > FB (Figure 7). This order was expected because the AM samples are thermodynamically metastable and as such should have a high dissolution rate, whereas the FB samples have a low solubility compared to the AM and DH samples and are therefore expected to have a lower dissolution rate. The change in dissolution rate of the AM sample was furthermore in accordance with the phase transformation kinetics suggested by the PCA plot of the Raman data. The changes in solid-state forms, detected by the combined application of UV imaging and Raman spectroscopy, occurring

during the dissolution of the AM and FB samples may well have been overlooked using the classical dissolution methods.

In summary, the UV imaging technique provides detailed information about the first minutes of a dissolution experiment. The ability to measure solution concentrations (absorbance) in the immediate vicinity of the surface of the dissolving material offers remarkably time-resolved dissolution rates. The spatial resolution of the UV images also provided an insight into the solid form changes occurring during dissolution. Thus UV imaging, particularly in combination with solid-state analysis, e.g., Raman spectroscopy, shows great potential in the study of drug dissolution processes and provides a new perspective to the in vitro testing of drug release.

■ ASSOCIATED CONTENT

Supporting Information. UV absorbance scan of amlodipine besylate; DSC thermogram, XPRD diffractogram, ^{1}H NMR spectrum, and TGA curve of amlodipine free base; and estimation of sensitivity of the UV imaging setup. This material is available free of charge via the Internet at http://pubs.acs.org.

■ AUTHOR INFORMATION

Corresponding Author

*Department of Pharmaceutics and Analytical Chemistry, Faculty of Pharmaceutical Sciences, University of Copenhagen, Universitetsparken 2, DK-2100 Copenhagen, Denmark. Tel: +45 35336138. Fax: +45 35336030. E-mail: joe@farma.ku.dk.

Present Addresses

‡Technical R&D, Novartis Pharma AG, CH-4056, Basel, Switzerland.

■ ACKNOWLEDGMENT

The work was supported by the Danish Medical Research Council and the Lundbeck Foundation. M.S. acknowledges support from the Academy of Finland (Researcher training and research abroad, decision number 137119).

■ REFERENCES

(1) Gardner, C. R.; Walsh, C. T.; Almarsson, O. Drugs as materials: valuing physical form in drug discovery. *Nat. Rev. Drug Discovery* **2004**, *3*, 926–934.

(2) Singhal, D.; Curatolo, W. Drug polymorphism and dosage form design: a practical perspective. *Adv. Drug Delivery Rev.* **2004**, *56*, 335–347.

(3) Cardew, P. T.; Davey, R. J. The Kinetics of Solvent-Mediated Phase Transformations. *Proc. R. Soc. London, Ser. A* **1985**, *398*, 415–428.

(4) Davey, R. J.; Cardew, P. T.; Mcewan, D.; Sadler, D. E. Rate Controlling Processes in Solvent-Mediated Phase-Transformations. *J. Cryst. Growth* **1986**, *79*, 648–653.

(5) Alonzo, D.; Zhang, G.; Zhou, D.; Gao, Y.; Taylor, L. Understanding the Behavior of Amorphous Pharmaceutical Systems during Dissolution. *Pharm. Res.* **2010**, *27*, 608–618.

(6) Mudie, D. M.; Amidon, G. L.; Amidon, G. E. Physiological Parameters for Oral Delivery and in Vitro Testing. *Mol. Pharmaceutics* **2010**, *7*, 1388–1405.

(7) Dressman, J. B.; Amidon, G. L.; Reppas, C.; Shah, V. P. Dissolution Testing as a Prognostic Tool for Oral Drug Absorption: Immediate Release Dosage Forms. *Pharm. Res.* **1998**, *15*, 11–22.

(8) Aaltonen, J.; Rades, T. Towards Physico-Relevant Dissolution Testing: The Importance of Solid-State Analysis in Dissolution. *Dissolution Technol.* **2009**, *16*, 47–54.

(9) Lehto, P.; Aaltonen, J.; Niemelä, P.; Rantanen, J.; Hirvonen, J.; Tanninen, V. P.; Peltonen, L. Simultaneous measurement of liquid-phase and solid-phase transformation kinetics in rotating disc and channel flow cell dissolution devices. *Int. J. Pharm.* **2008**, *363*, 66–72.

(10) Lehto, P.; Aaltonen, J.; Tenho, M.; Rantanen, J.; Hirvonen, J.; Tanninen, V. P.; Peltonen, L. Solvent-mediated solid phase transformations of carbamazepine: Effects of simulated intestinal fluid and fasted state simulated intestinal fluid. *J. Pharm. Sci.* **2009**, *98*, 985–996.

(11) Pal, A.; Indireshkumar, K.; Schwizer, W.; Abrahamsson, B.; Fried, M.; Brasseur, J. G. Gastric flow and mixing studied using computer simulation. *Proc. R. Soc. London, Ser. B* **2004**, *271*, 2587–2594.

(12) Abrahamsson, B.; Albery, T.; Eriksson, A.; Gustafsson, I.; Sjoberg, M. Food effects on tablet disintegration. *Eur J. Pharm. Sci.* **2004**, *22*, 165–172.

(13) Abrahamsson, B.; Pal, A.; Sjoberg, M.; Carlsson, M.; Laurell, E.; Brasseur, J. G. A novel in vitro and numerical analysis of shear-induced drug release from extended-release tablets in the fed stomach. *Pharm. Res.* **2005**, *22*, 1215–1226.

(14) McAllister, M. Dynamic Dissolution: A Step Closer to Predictive Dissolution Testing? *Mol. Pharmaceutics* **2010**, *7*, 1374–1387.

(15) Tong, C.; D'Souza, S.; Parker, J.; Mirza, T. Commentary on AAPS Workshop. *Pharm. Res.* **2007**, *24*, 1603–1607.

(16) Tong, C.; Lozano, R.; Mao, Y.; Mirza, T.; Löbenberg, R.; Nickerson, B.; Gray, V.; Wang, Q. The Value of In Vitro Dissolution in Drug Development. *Pharm. Technol.* **2009**, *33*, 52–64.

(17) Azarmi, S.; Roa, W.; Löbenberg, R. Current perspectives in dissolution testing of conventional and novel dosage forms. *Int. J. Pharm.* **2007**, *328*, 12–21.

(18) Gray, V.; Kelly, G.; Xia, M.; Butler, C.; Thomas, S.; Mayock, S. The Science of USP 1 and 2 Dissolution: Present Challenges and Future Relevance. *Pharm. Res.* **2009**, *26*, 1289–1302.

(19) Dokoumetzidis, A.; Macheras, P. A century of dissolution research: From Noyes and Whitney to the Biopharmaceutics Classification System. *Int. J. Pharm.* **2006**, *321*, 1–11.

(20) Aaltonen, J.; Heinänen, P.; Peltonen, L.; Kortejärvi, H.; Tanninen, V. P.; Christiansen, L.; Hirvonen, J.; Yliruusi, J.; Rantanen, J. In situ measurement of solvent-mediated phase transformations during dissolution testing. *J. Pharm. Sci.* **2006**, *95*, 2730–2737.

(21) Amidon, G. E.; Hawley, M. Oral Bioperformance and 21st Century Dissolution. *Mol. Pharmaceutics* **2010**, *7*, 1361–1361.

(22) Coutts-Lendon, C. A.; Wright, N. A.; Mieso, E. V.; Koenig, J. L. The use of FT-IR imaging as an analytical tool for the characterization of drug delivery systems. *J. Controlled Release* **2003**, *93*, 223–248.

(23) Nott, K. P. Magnetic resonance imaging of tablet dissolution. *Eur. J. Pharm. Biopharm.* **2010**, *74*, 78–83.

(24) Kazarian, S. G.; Chan, K. L. A. Applications of ATR-FTIR spectroscopic imaging to biomedical samples. *Biochim. Biophys. Acta* **2006**, *1758*, 858–867.

(25) Reich, G. Near-infrared spectroscopy and imaging: basic principles and pharmaceutical applications. *Adv. Drug Delivery Rev.* **2005**, *57*, 1109–43.

(26) Kassis, A.; Bhawtankar, V. M.; Sowa, J. R. Attenuated total reflection infrared spectroscopy (ATR-IR) as an in situ technique for dissolution studies. *J. Pharm. Biomed. Anal.* **2010**, *53*, 269–273.

(27) van der Weerd, J.; Andrew Chan, K. L.; Kazarian, S. G. An innovative design of compaction cell for in situ FT-IR imaging of tablet dissolution. *Vib. Spectrosc.* **2004**, *35*, 9–13.

(28) Zumbusch, A.; Holtom, G. R.; Xie, X. S. Three-Dimensional Vibrational Imaging by Coherent Anti-Stokes Raman Scattering. *Phys. Rev. Lett.* **1999**, *82*, 4142.

(29) Windbergs, M.; Jurna, M.; Offerhaus, H. L.; Herek, J. L.; Kleinebudde, P.; Strachan, C. J. Chemical imaging of oral solid dosage forms and changes upon dissolution using coherent anti-Stokes Raman scattering microscopy. *Anal. Chem.* **2009**, *81*, 2085–2091.

(30) Cheng, J. X.; Volkmer, A.; Xie, X. S. Theoretical and experimental characterization of coherent anti-Stokes Raman scattering microscopy. *J. Opt. Soc. Am. B* **2002**, *19*, 1363–1375.

(31) Saar, B. G.; Freudiger, C. W.; Reichman, J.; Stanley, C. M.; Holtom, G. R.; Xie, X. S. Video-Rate Molecular Imaging in Vivo with Stimulated Raman Scattering. *Science* **2010**, *330*, 1368–1370.

(32) Østergaard, J.; Meng-Lund, E.; Larsen, S. W.; Larsen, C.; Petersson, K.; Lenke, J.; Jensen, H. Real-time UV imaging of nicotine release from transdermal patch. *Pharm. Res.* **2010**, *27*, 2614–23.

(33) Østergaard, J.; Ye, F.; Rantanen, J.; Yaghmur, A.; Larsen, S. W.; Larsen, C.; Jensen, H. Monitoring Lidocaine Single-Crystal Dissolution by Ultraviolet Imaging. *J. Pharm. Sci.* **2011**, DOI 10.1002/jps.22532.

(34) Tian, F.; Zeitler, J. A.; Strachan, C. J.; Saville, D. J.; Gordon, K. C.; Rades, T. Characterizing the conversion kinetics of carbamazepine polymorphs to the dihydrate in aqueous suspension using Raman spectroscopy. *J. Pharm. Biomed. Anal.* **2006**, *40*, 271–280.

(35) Greco, K.; Bergman, T. L.; Bogner, R. Design and characterization of a laminar flow-through dissolution apparatus: Comparison of hydrodynamic conditions to those of common dissolution techniques. *Pharm. Dev. Technol.* **2011**, *16* (1), 75–87.

(36) Greco, K.; McNamara, D. P.; Bogner, R. Solution-mediated phase transformation of salts during dissolution: Investigation using haloperidol as a model drug. *J. Pharm. Sci.* **2011**, *100* (7), 2755–2768.

(37) Tian, F.; Sandler, N.; Aaltonen, J.; Lang, C.; Saville, D. J.; Gordon, K. C.; Strachan, C. J.; Rantanen, J.; Rades, T. Influence of polymorphic form, morphology, and excipient interactions on the dissolution of carbamazepine compacts. *J. Pharm. Sci.* **2007**, *96*, 584–594.

(38) Missel, P. J.; Stevens, L. E.; Mauger, J. W. Reexamination of convective diffusion/drug dissolution in a laminar flow channel: Accurate prediction of dissolution rate. *Pharm. Res.* **2004**, *21*, 2300–2306.

(39) Compton, R. G.; Pritchard, K. L.; Unwin, P. R. The Direct Measurement of Dissolution Kinetics at the Calcite Water Interface. *J. Chem. Soc., Chem. Commun.* **1989**, 249–251.

(40) Brown, C. A.; Compton, R. G.; Narramore, C. A. The Kinetics of Calcite Dissolution Precipitation. *J. Colloid Interface Sci.* **1993**, *160*, 372–379.

(41) Shah, A. C.; Nelson, K. G. Evaluation of a Convective Diffusion Drug Dissolution Rate Model. *J. Pharm. Sci.* **1975**, *64*, 1518–1520.

(42) Savolainen, M.; Kogermann, K.; Heinz, A.; Aaltonen, J.; Peltonen, L.; Strachan, C.; Yliruusi, J. Better understanding of dissolution behaviour of amorphous drugs by in situ solid-state analysis using Raman spectroscopy. *Eur. J. Pharm. Biopharm.* **2009**, *71*, 71–79.

(43) Threlfall, T. L. Analysis of organic polymorphs. A review. *Analyst* **1995**, *120*, 2435–2460.

(44) Bugay, D. E. Characterization of the solid-state: spectroscopic techniques. *Adv. Drug Delivery Rev.* **2001**, *48*, 43–65.

(45) Pelletier, M. Quantitative Analysis Using Raman Spectrometry. *Appl. Spectrosc.* **2003**, *57*, 20A–42A.

(46) Svensson, O.; Josefson, M.; Langkilde, F. W. Reaction monitoring using Raman spectroscopy and chemometrics. *Chemometr. Intell. Lab. Syst.* **1999**, *49*, 49–66.

(47) Hu, Y.; Liang, J. K.; Myerson, A. S.; Taylor, L. S. Crystallization Monitoring by Raman Spectroscopy: Simultaneous Measurement of Desupersaturation Profile and Polymorphic Form in Flufenamic Acid Systems. *Ind. Eng. Chem. Res.* **2004**, *44*, 1233–1240.

(48) Koradia, V.; de Diego, H. L.; Frydenvang, K.; Ringkjobing-Elema, M.; Mullertz, A.; Bond, A. D.; Rantanen, J. Solid Forms of Amlodipine Besylate Physicochemical, Structural, and Thermodynamic Characterization. *Cryst. Growth Des.* **2010**, *10*, 5279–5290.

(49) Rollinger, J. M.; Burger, A. Physico-chemical characterization of hydrated and anhydrous crystal forms of amlodipine besylate. *J. Therm. Anal. Calorim.* **2002**, *68*, 361–372.

(50) Clayton, B. R.; Massey, B. S. Flow Visualization in Water—a Review of Techniques. *J. Sci. Instrum.* **1967**, 44.

(51) Koradia, V.; Fontelonga de Lemos, A. F.; Allesø, M.; Lopez de Diego, H.; Ringkjøbing-Elema, M.; Müllertz, A.; Rantanen, J. Phase transformations of amlodipine besylate solid forms. *J. Pharm. Sci.* **2011**, *100*, 2896–2910.

(52) Chan, K. L. A.; Fleming, O. S.; Kazarian, S. G.; Vassou, D.; Chryssikos, G. D.; Gionis, V. Polymorphism and devitrification of nifedipine under controlled humidity: a combined FT-Raman, IR and Raman microscopic investigation. *J. Raman Spectrosc.* **2004**, 35, 353–359.

(53) Lemmens, J. M.; Peters, T. H. A.; Benneker, F. B. G.; Keltjens, R. Amlodipine free base. United States Patent 7,335,380, 2001.

(54) Van Eerdenbrugh, B.; Alonzo, D.; Taylor, L. Influence of Particle Size on the Ultraviolet Spectrum of Particulate-Containing Solutions: Implications for In-Situ Concentration Monitoring Using UV/Vis Fiber-Optic Probes. *Pharm. Res.* **2011**, 1–10.